

# Roles of Friction-Induced Strain Hardening and Recrystallization in Dry Sliding Wear of AZ31 Magnesium Alloy

C. Liang · X. Han · T. F. Su · X. X. Lv · J. An

Received: 15 March 2014 / Accepted: 15 July 2014 / Published online: 15 October 2014  
© The Indian Institute of Metals - IIM 2014

**Abstract** Dry sliding wear tests were performed on AZ31 alloy using a pin-on-disc configuration under the loads of 5–360 N and sliding speeds of 0.1–1.5 m/s. Friction and wear characteristics of AZ31 alloy were investigated as a function of the load and sliding speed. Wear mechanisms for AZ31 alloy were characterized by scanning electron microscopy. The wear behavior in mild and severe wear regimes was described in terms of plastic deformation and microstructure evolution in subsurface, and surface hardness change and temperature rise of worn surfaces. The results revealed that surface strain hardening caused by large plastic deformation played an important role in maintaining a low slope of wear rate in mild wear regime, while surface thermal softening originating from dynamic recrystallization and surface melting were responsible for a rapid wear in severe wear regime.

**Keywords** AZ31 alloy · Strain hardening · Dynamic recrystallization · Sliding wear · Wear mechanism

## 1 Introduction

Magnesium alloys have been widely used in the electronics, aerospace and automotive industries due to their attractive properties such as low density, high specific strength, damping capacity and good electrical and thermal conductivity [1–3]. However, poor wear resistance and low

strength at elevated temperatures are serious impediments against their being used as widely as Al alloys in applications requiring high strength at elevated temperatures, such as automotive engine components including pistons and cylinder liners. They are also a major reason that only limited wear investigations so far have been carried out on magnesium alloys as compared with aluminum alloys. Recently, many processing techniques have been employed to improve mechanical properties of Mg alloys at elevated temperatures, such as rare earth elements alloying, rapidly solidified powder metallurgy (RS P/M) and reinforcing the Mg alloy matrix with hard nano-sized ceramic particles. As a consequence, a number of magnesium alloys with excellent elevated temperature mechanical properties have been developed. Janik et al. [4] applied peak-ageing treatment to Mg-10Gd-3Y-0.4Zr alloy, which has the ultimate tensile stresses and compressive peak stresses above 300 MPa at temperatures up to 250 °C. Kawamura et al. [5] and Inoue et al. [6] developed the Mg<sub>97</sub>Zn<sub>1</sub>Y<sub>2</sub> RS P/M alloy, which has high strength above 600 MPa at ambient temperature and excellent yield strength of 510 MPa at 150 °C. Habibnejad-Korayem et al. [7] prepared an AZ31 Mg-based composite reinforced with 2 wt% Al<sub>2</sub>O<sub>3</sub> nano-particles, the nano-composite presents improved wear behavior by the enhanced work-hardening capability arising from interaction of dislocations and nano-particles. All the achievements inspire the growing interest in wear behavior of magnesium alloys. Most investigations mainly focus on transitions of wear rate and wear mechanism with applied load or sliding speed, and the consequent establishments of wear rate map and wear transition map. Chen and Alpas [8] found that the mild to severe wear transition for AZ91 alloy was controlled by the contact surface temperature criterion, i.e. the onset of the severe wear was coincided with a surface temperature of

C. Liang · X. Han · T. F. Su · X. X. Lv (✉) · J. An  
Key Laboratory of Automobile Materials, Ministry of Education,  
Department of Materials Science and Engineering, Jilin  
University, Changchun 130025, People's Republic of China  
e-mail: lvxiaoxiaju2000@163.com

74 °C. They divided the sliding wear map for AZ91 into two regimes, i.e. the mild wear regime and severe wear regime. The mild wear regime consisted of two sub-wear regimes, namely an oxidation wear regime and a delamination wear regime; the severe wear regime comprised a severe plastic deformation wear regime and a melt wear regime. Analogous wear investigations were also undertaken on hot deformed AZ61 alloy by El-Morsy [9], AM60 alloy by Taltavull et al. [10], Mg-Sn based alloys by Poddar et al. [11], and as-cast and hot extruded ZE41 alloy by Anbu selvan and Ramanathan [12].

Sliding contact between ductile materials often induces plastic deformation in the near-surface region [13]. The combination of plastic deformation and frictional heating in the near-surface region play a significant role in microstructural evolution and mechanical change, which conversely influence the external wear behaviour including variations in coefficient of friction and wear rate, and wear mechanism transition. Up to date, very few works have been systematically performed on friction induced microstructure evolution, strain hardening, dynamic recrystallization (DRX) in the near-surface region as well as consequent influence on wear behavior of magnesium alloys. Das et al. [14] investigated the microstructural evolution during high temperature sliding wear of AZ31 alloy mostly at 400 °C. They found that the wear mechanism transformed from oxidation into severe plastic deformation when the ambient temperature is increased from low temperature to high temperature ( $T > 300$  °C), the subsurface material also experienced DRX, grain growth, and grain boundary sliding occurred at the edges of the wear tracks. Somekava et al. [15] studied the microstructural evolution near the surface region during dry sliding wear test in magnesium and Mg-Y alloy. They found that the plastic deformation occurred even at the beginning of the test, the deformed microstructures of both alloys consisted of {10–12} twinning formation, and the superior friction and wear resistance of Mg-Y alloy was due to the suppression of material softening i.e. grain refinement and grain boundary sliding originating from DRX. The effect of DRX in subsurface on wear behavior is also identified in other metallic materials. Yao et al. [16] investigated the worn subsurface structure evolution in pure copper specimens with various microstructures, and identified the correlation that wear rate increases significantly with an increasing grain size or a decreasing hardness of the DRX structure adjacent to the top nanostructured mixing layer.

The strong correlation between evolutions of microstructure and mechanical properties in subsurface and wear behaviour has not been elucidated in detail, specifically, the roles of surface hardening originating from plastic deformation and subsurface recrystallisation induced by

frictional heating in wear of magnesium alloys. In the present work, as cast AZ31 magnesium alloy was chosen as material to study in consideration two aspects: (i) the small amount of  $Al_{17}Mg_{12}$  and  $Al_8Mn_5$  particles in as-cast AZ31 alloy has little influence on microstructural evolution during sliding, and the as-cast condition of AZ31 alloy can provide quite clear grains free from deformation twins for observation of subsurface deformation. (ii) AZ31 alloy is a widely used wrought magnesium alloy which can be processed by rolling, extrusion, forging etc., the friction-induced subsurface microstructural evolution and hardness change is helpful to better understand the corresponding changes in deformed material at the work-tool interface. The roles of friction-induced strain hardening and DRX in wear behavior of AZ31 were thoroughly investigated via plastic deformation measurement, microstructure observation and hardness test.

## 2 Experimental

### 2.1 Testing Material

The material used in this work was a commercial AZ31 alloy ingot with the nominal chemical composition of Mg-3.0Al-1.0Zn-0.2Mn (in mass%). The microstructure of AZ31 ingot consisted of coarse  $\alpha$ -Mg solid solution grains and fine intermetallic particles, as shown in Fig. 1. Grain size of  $\alpha$ -Mg phase  $d$  was measured by the liner intercept method using the equation  $d = 1.74 L$ , where  $L$  is the liner interception size. The average grain size of  $\alpha$ -Mg phase was around 157  $\mu\text{m}$ . Two types of intermetallic phases that precipitated in the forms of rod and sphere within the grain and on boundaries of  $\alpha$ -Mg solid solution were identified as  $Al_8Mn_5$  and  $Mg_{17}(AlZn)_{12}$  by energy dispersive X-ray spectrometer (EDS). Rod-shaped particles correspond to  $Al_8Mn_5$  phase, sphere particles belong to  $Mg_{17}(AlZn)_{12}$  phase. The corresponding compositions of two types of intermetallic particles measured by EDS are listed in Table 1, in which the measured atomic ratio of Al to Mn for  $Al_8Mn_5$  phase is 1.74, close to 1.6, the theoretical atomic ratio of Al to Mn in  $Al_8Mn_5$  phase, and the measured atomic ratio of Mg to Al + Zn for  $Mg_{17}(AlZn)_{12}$  phase is 1.45, close to 1.42, the theoretical atomic ratio of Mg to Al + Zn in  $Mg_{17}(AlZn)_{12}$  phase. Microhardness of the alloy was measured as about 51 on Vickers scale using a load of 100 gf for a dwell period of 20 s as per ASTM E384-06 standard.

Thermal transformations in the as cast AZ31 alloy were examined using differential thermal analysis (DTA). During continuous heating of AZ31 alloy, endothermic peak appeared with an onset temperature of 241 °C, corresponding to dissolution of  $\beta$ - $Mg_{17}(AlZn)_{12}$  precipitate

phase, endothermic peak appeared with an onset temperature of 591 °C, corresponding to melting of  $\alpha$ -Mg phase.

## 2.2 Sliding Wear Test

Friction and wear tests were conducted with a pin-on-disc type machine under dry sliding condition at a room temperature of 25 °C. Specimens of 6 mm diameter  $\times$  13 mm length were machined from the commercial AZ31 alloy ingot. Before the commencement of each wear test, specimen surfaces were thoroughly degreased by acetone and dried. The tests were carried out in an applied load range of 5–360 N and at sliding speeds of 0.1, 0.785 and 1.5 m/s, respectively. The constant sliding distance was 377 m (2,000 cycles). The mass losses were calculated from the difference in weight of specimens measured before and after the wear test using a precision pan electrical balance (0.0001 g). Volumetric wear rate was calculated by dividing the volumetric wear loss by sliding distance. The disc was 70 mm in diameter and made of high carbon chromium steel hardened to 57 HRC, the bearing surface of which was ground to a constant surface roughness of about 0.4  $\mu$ m Ra. Worn surfaces of the pins were examined with a JSM-5600 scanning electron microscope (SEM) equipped with an EDS.

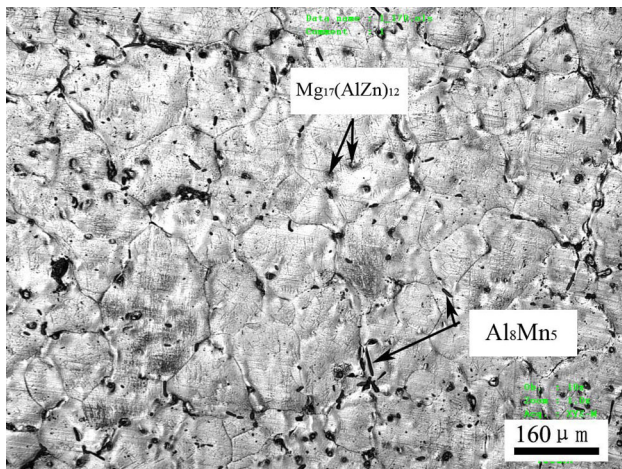


**Fig. 1** Microstructure of as cast AZ31 alloy

**Table 1** Compositions of two types of intermetallic phases by EDS

Intermetallic phase	Content	MgK	AlK	MnK	ZnK
Al <sub>8</sub> Mn <sub>5</sub>	Weight percent	4.12	43.79	51.07	1.03
	Atomic percent	6.18	59.28	33.96	0.58
Mg <sub>17</sub> (AlZn) <sub>12</sub>	Weight percent	49.38	29.79	1.53	19.3
	Atomic percent	58.73	31.92	0.81	8.54

## 2.3 Subsurface Microstructure Observation and Surface Hardness Test

Observation of microstructural evolution in subsurface was performed on cross sections of worn pins under a LEXT-OLS3000 confocal scanning laser microscope. The metallographic samples were prepared by cutting worn pins into two parts along the sliding direction, mounted in epoxy resin, and then prepared by the standard metallographic method, following by ASTM E3-2001 standard. The surface microhardness of worn pins was measured on Vickers scale using a load of 100 gf for a dwell period of 20 s as per ASTM E384-06 standard; each hardness value was obtained from an average of at least three test results.

## 3 Results and Discussion

### 3.1 Wear Behavior

The coefficient of friction and wear rate of AZ31 alloy are plotted against applied load for the tests conducted at a constant sliding speed of 0.1, 0.785 and 1.5 m/s in Fig. 2a, b respectively. At the three sliding speeds, the coefficients of friction of AZ31 alloy did not differ much from each other, and interweaved at certain loads. With increasing load, the coefficient of friction exhibited a clear decreasing trend, which could be divided into two regions distinguished according to the difference in the slope of the coefficient of friction versus applied load plot, i.e., the first region was in the load range of 5–30 N, corresponding to a sharp drop in coefficient of friction from about 1.0 to 0.5 due to improvement of the contact surface; the second region was in the load range of 30–360 N at 0.1 m/s, 30–360 N at 0.785 m/s, and 30–190 N at 1.5 m/s, corresponding to a gentle decrease in coefficient of friction from about 0.5–0.3 at 0.1 m/s due to the increase in the real contact area, 0.5–0.25 at 0.785 m/s and 0.5–0.38 at 1.5 m/s due to the activation of additional slip planes, thermal softening and surface melting in the near-surface layer of AZ31 alloy with increased frictional heating.

It is noticed that there is a great difference in wear rates between the tests at the three sliding speeds. When the load was less than 30 N, wear rates at three sliding speeds all

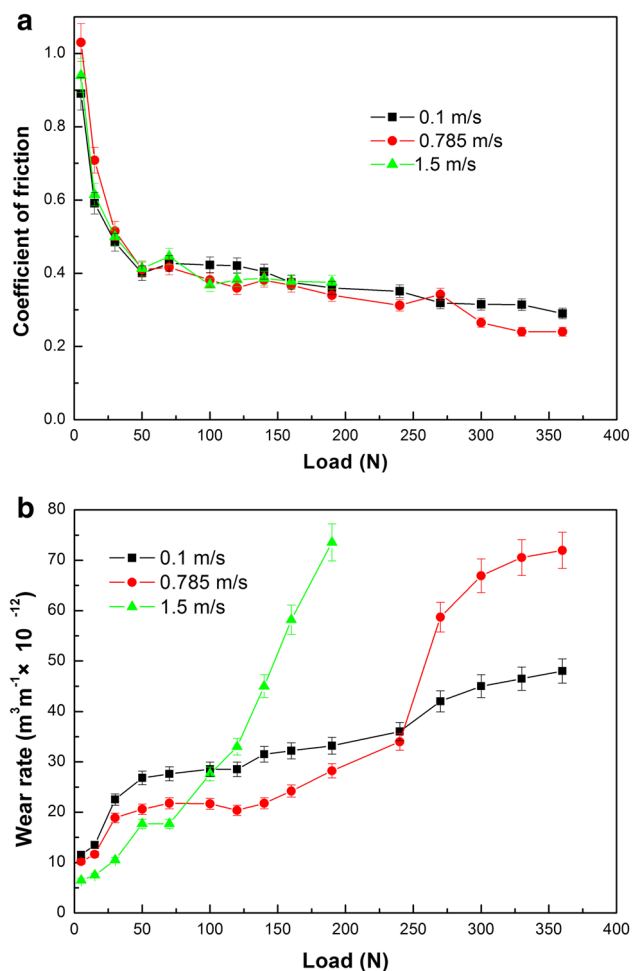


**Fig. 2** Variation in coefficient of friction (a) and wear rate (b) with load for AZ31 alloy at different sliding speeds

presented a low level of value between  $5$  to  $14 \times 10^{-12} \text{ m}^3 \text{ m}^{-1}$ , and higher sliding speed showed low wear rate. This reduction in wear rate with increasing sliding speed at lower loads is mainly attributed to friction heating. As the sliding speed increased, frictional heating causes surface temperature to rise, activating additional slip planes thereby promoting greater ductility of material in the near-surface layer. In addition, increasing sliding speed also promotes formation of oxide film on worn surface, which is beneficial in reducing true metallic contact of the wearing surfaces. These can be the causes for the decline in wear rate with increasing sliding speed at lower loads. Nguyen et al. [17] also observed similar phenomenon in wear of AZ31B alloy. They found that with increasing sliding speed from 1.0 m/s to 5.0 m/s under 10 N, the wear rate of AZ31B alloy decreased. When the load was higher than 30 N, wear rates of AZ31 alloy at three sliding speeds differed greatly from each other. At 0.1 m/s, the wear rate slightly increased in an almost linear relationship with applied load throughout the load range of 30–360 N,

whereas at sliding speeds of 0.785 and 1.5 m/s, the slightly increasing region of wear rate was restricted within a narrow load range, i.e. 30–120 N at 0.785 m/s and 50–70 N at 1.5 m/s, hereafter followed by two sequent rapidly increasing regions of wear rate within 120–240 and 240–360 N at 0.785 m/s, and a linearly increasing region of wear rate within 70–180 N at 1.5 m/s. Large changes in the slopes of the wear rate versus load curves occurred at 120 N and at 0.785 m/s, and at 70 N and at 1.5 m/s, indicating that the wear transforms from mild wear to severe wear at the two transition loads. Severe wear is typically characterized by massive surface damage and production of large metallic debris particles, two types of materials removal wear mechanisms usually operates within the severe wear regime as the load condition changes, namely severely plastic deformation of the material layers adjacent to the contact surface and friction-induced melting. The wear rates of AZ31 alloy at the transition loads of 140 and 70 N were about  $21 \times 10^{-12}$  and  $18 \times 10^{-12} \text{ m}^3 \text{ m}^{-1}$ , which were a little lower than the wear rates of  $26 \times 10^{-12}$  and  $18.5 \times 10^{-12} \text{ m}^3 \text{ m}^{-1}$  at transition loads of 180 and 80 N when sliding at 0.5 and 1.5 m/s for dry wear tests conducted on AZ91 alloy by Chen and Alpas [8].

Five wear mechanisms were observed operating in different load ranges under the three sliding conditions, they were oxidation, abrasion, delamination, thermal softening and surface melting. Oxidation, abrasion and delamination operated in mild wear regime, while thermal softening and surface melting worked in severe wear regime. The wear mechanisms of AZ31 alloy conform well to those observed in other magnesium alloys [8–12]. The load ranges of wear mechanism operating at different sliding speeds for AZ31 alloy are summarized in Table 2. At low sliding speed of 0.1 m/s, only three wear mechanisms, i.e., oxidation, abrasion and delamination were observed, in which delamination controlled throughout the load range of 30–360 N. At high sliding speeds of 0.785 and 1.5 m/s, five wear mechanisms with typical worn surface morphologies were observed separately in different load ranges. Figure 3 shows the typical characteristics of worn surface morphologies in different wear mechanisms for AZ31 alloy at the sliding speed of 0.785 m/s.

### 3.2 Subsurface Plastic Deformation and Strain Hardening

It is noticed that at the three sliding speeds, the tested material exhibits a low slope on wear rate versus applied load curves in the load ranges of 30–360, 30–120 and 50–70 N, respectively. The wear rate shows a relatively small dependence on applied load within these load ranges. To explain this phenomenon occurring in mild wear

**Table 2** Load ranges of wear mechanism operating at different sliding speeds

Sliding speed (m/s)	Oxidation	Abrasion	Delamination	Thermal softening	Surface melting
0.1	5–30	5–30	30–360	–	–
0.785	5–30	5–30	30–120	120–240	240–360
1.5	5–50	5–50	50–70	70–120	120–190

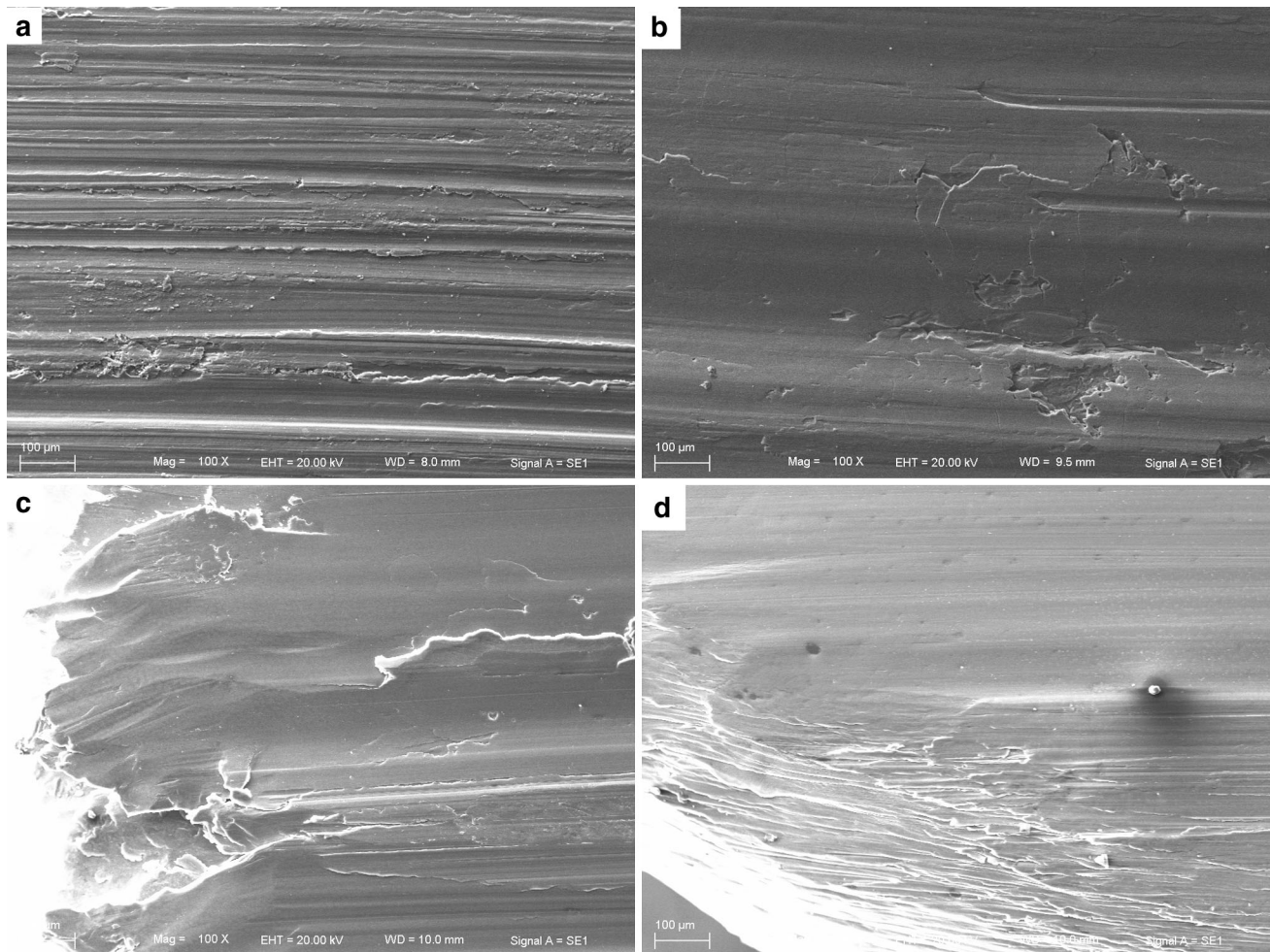


**Fig. 3** SEM micrographs of test pin surfaces of AZ31 alloy at different applied loads under 0.785 m/s: **a** oxidation and abrasion, showing grooves and oxidative powders at 15 N, **b** delamination, showing cracks at 120 N, **c** thermal softening, showing extruded layers of pin surface edge at 190 N, **d** surface melting, showing re-solidified layers of the pin surface edge at 270 N

regime, analyses were conducted from three aspects including surface oxidation, subsurface deformation and surface hardness. Oxidation film induced by tribochemical reaction of Mg and O and mechanically mixed layer (MML) formed on worn surfaces of magnesium alloys usually exhibit higher hardness than substrates of Mg alloys; consequently formation of such an oxidation film or MML on pin surface can improve wear resistance. As reported by our previous study on wear behavior of AZ91 alloy, formation of a cell-network structure oxidation film caused a sudden drop in wear rate [18]. Wang et al. [19]

found that MML formed on AZ91 alloy had a high hardness of 110–120 HV, which reduced the wear remarkably under a low load range of 12.5–25 N when the wear test temperature was in a range of 25–200 °C. The content of O element on worn surfaces subjected to different sliding speeds is measured by EDS, and plotted in Fig. 4 as a function of applied load. It revealed no high content of O element found on worn surfaces of AZ31 alloy in aforementioned load ranges with low slope of wear rates shown in Fig. 2b. For example, in case of pins sliding at 0.785 m/s, the content of O element was as high as about

14.9–17.9 wt% in low load range of 10–30 N, then reduced to about 6.82 at 50 N and 6.9 wt% at 70 N, respectively. In case of pins sliding at 1.5 m/s, the content of O element was as high as about 15.93 wt% at 15 N, and then reduced to 3.85 wt% at 70 N and 3.43 wt% at 140 N, respectively. In addition, no evidence of dense oxidation film or MML could be clearly observed on worn surfaces or cross-sections of the pins in delamination wear regime. Therefore, it suggests that the surface oxidation plays an important role in keeping a low wear rate within the load range of 5–30 N on wear rate curves, but not a dominant role in maintaining a low slope of wear rate when the applied load is beyond 50 N.

The plastic shear deformation in subsurface was characterized by equivalent plastic shear strain distribution beneath the worn surface. The variation of plastic shear strain as a function of depth from the worn surface was calculated using the curvature of the flow lines described by Moore and Douthwaite [20]. The equivalent plastic strain at a depth  $z$  beneath the worn surface can be calculated from the shear angle of the interface,  $\theta$ , as follows:

$$\varepsilon(z) = \frac{\sqrt{3}}{3} \tan(\theta(z)) \quad (1)$$

The experimentally determined equivalent plastic strain distributions beneath the worn surfaces at loads of 15, 70 and 120 N under sliding speed of 0.785 m/s are shown in Fig. 5. The subsurface plastic strains beneath the worn surfaces varies in a similar way at the three applied loads, they all drop remarkably within a depth range of 5–60  $\mu\text{m}$ , and then decrease gradually with further increasing the depth. Under the three applied loads, the plastic strains reached as high as 300–400 % at depth less than 5  $\mu\text{m}$ , and still exceeded 100 % at depth of about 40  $\mu\text{m}$ . Even at a low load of 15 N, a large plastic strain was induced in the

near-surface region. In order to understand the plastic strain accumulation process in subsurface before mild to severe wear transition, the effect of sliding cycle on friction-induced plastic strain distribution was investigated on pins subjected to 120 N, i.e. the mild to severe wear transition load, as shown in Fig. 6. The plastic strain reached as high as 324 % at depth less than 5  $\mu\text{m}$  even after sliding only 100 cycles. With increasing sliding cycle, the near-surface region with large plastic strain continued to widen until 1,400 cycles, at which a steady plastic strain distribution was established as the difference in the plastic strain distributions is almost negligible after sliding 1,400 and 2,000 cycles. Such large strain accumulation in subsurface may induce either surface strain hardening or softening originating from DRX during sliding wear tests, depending on the worn surface temperature rise during dry sliding wear test.

Since the combination of applied load and friction force can cause substantial plastic deformation in subsurface, the surface strain hardening is inevitable during sliding wear test, and hence counteracts the effect of increasing load on wear rate, to a great certain extent. After sliding at three speeds, the worn surface hardness is plotted as a function of applied load in Fig. 7. It can be seen that the surface hardness starts increasing rapidly even at low load range of 5–15 N under the three sliding conditions, and then it develops into different manners with respect to sliding speed. At 0.1 m/s, the surface hardness maintains a high level of 114–136 HV throughout the applied load range. At 0.785 m/s, the surface hardness reaches the highest level of 120–140 HV within 30–120 N, then dramatically drops to 110–115 HV within 120–240 N, and finally decreases to the lowest level of 100–107 HV within 240–360 N. From the surface hardness curves, The onset loads for surface hardness sudden drop were 120 N at 0.785 m/s and 70 N at

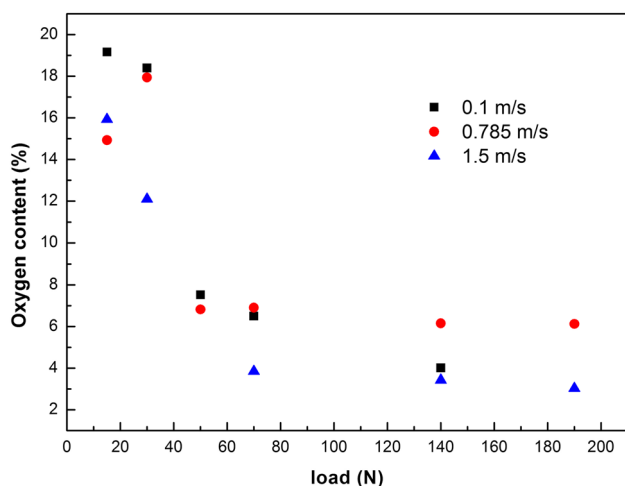


**Fig. 4** Oxygen content versus applied load at different sliding speeds

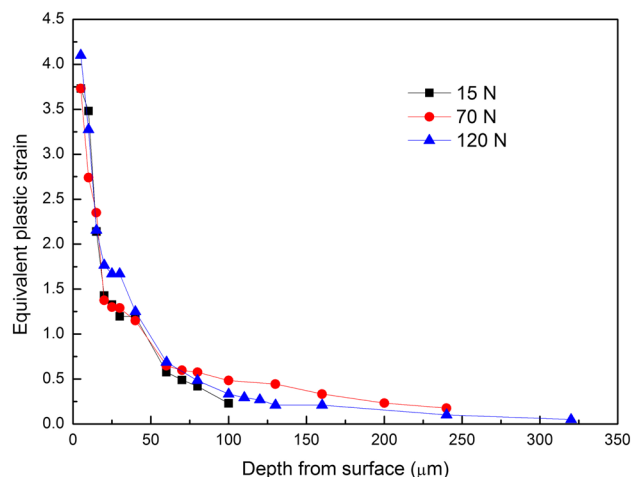


**Fig. 5** Variation of equivalent plastic strain as a function of depth from surface for samples tested at 15, 70 and 140 N under 0.785 m/s

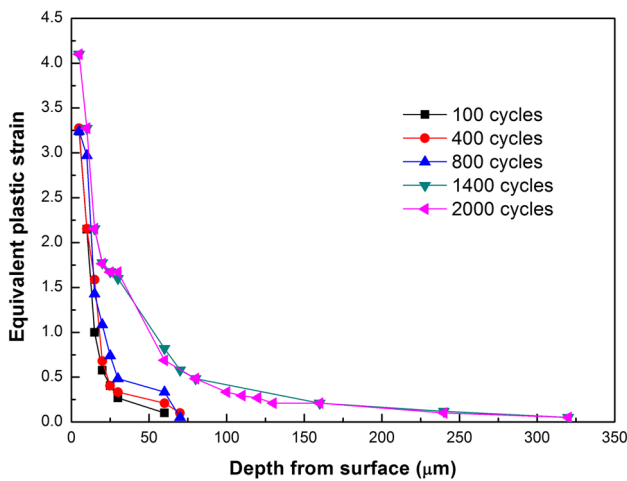


**Fig. 6** Equivalent plastic strain distributions in subsurfaces at 120 N under 0.785 m/s after different sliding cycles

1.5 m/s respectively, which agree well with the transition loads identified from the wear rate versus load curves shown in Fig. 2b. An interesting phenomenon is observed that there is a dip at a constant load of 50 N on hardness versus applied load curves regardless of the sliding speed, and then the hardness rises up more or less again when the load is above 50 N. It is presumed that the constant load of 50 N may be the critical load for the spallation or removal of the surface oxidation film. In order to confirm this point of view, analyses were carried on elemental mappings of O element and the chemical compositions of worn surfaces under different sliding conditions by SEM and EDS. Elemental mappings of O exhibits a decrease in coverage of oxide film when applied was increased from 10 to 50 N (not shown here). From the contents of O element on worn surfaces subjected to different loads and sliding speeds shown in Fig. 4, it can be seen that worn surface exhibits the highest O element content of about 12–19 % in the load range of 10–30 N, but a low O element of about 6–7 % at load of 50 N. Therefore, the load of 50 N may be the critical load for removal of the oxidation film from surfaces under sliding speeds of 0.1, 0.785 and 1.5 m/s.

Considering that the surface oxidation extent is rather low when the load is larger than 50 N, the high surface hardness possibly results from strain hardening within the load ranges of 50–360 N under 0.1 m/s and 50–120 N under 0.785 m/s. The low surface hardness within 120–140 N at 0.785 m/s is probably due to the transformation from a deformed microstructure into a DRX microstructure in subsurface.

### 3.3 Subsurface Dynamic Recrystallisation

Since large plastic strain is accumulated in the near-surface region even at a low load of 15 N, the surface temperature

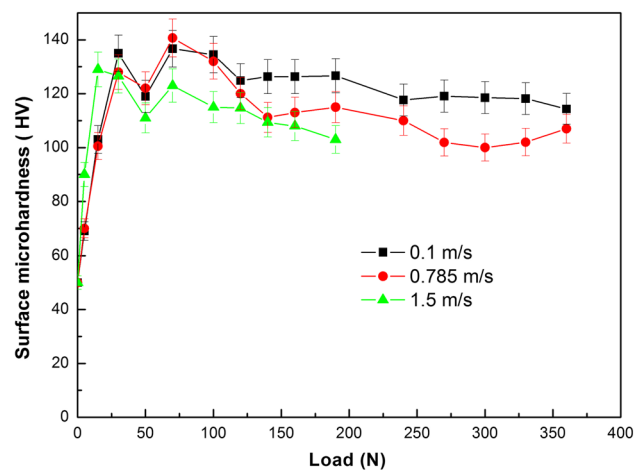


**Fig. 7** Hardness of worn surfaces of pins subjected to different sliding speeds and loads

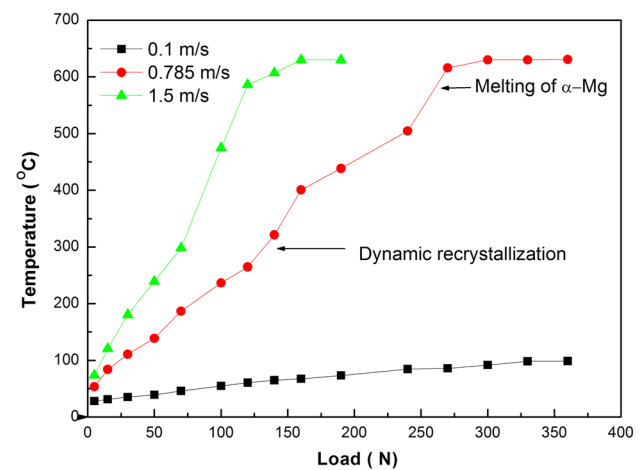


**Fig. 8** Variations in surface temperature with applied load at different sliding speeds

rising during dry sliding wear test is a dominant factor for realization of DRX in subsurface. The DRX initiates at about 300 °C for AZ31 alloy [21, 22]

Surface temperature rise can not be accurately measured by thermocouple probe because the whole pin surface is kept in close contact with disc and the temperature gradient is very large in axial direction of pin. Therefore, the surface temperature of pin during sliding was evaluated in a manner described by Lim and Ashby [23]. The average surface temperature  $T_b$  in sliding contact can be expressed as

$$T_b = T_0 + \frac{\alpha \mu F v l_b}{A_n K_{mp}} \quad (2)$$

$$\alpha = \frac{1}{2 + \frac{K_{md}}{K_{mp}} l_b (\pi v / 8 a r_0)^{1/2}} \quad (3)$$

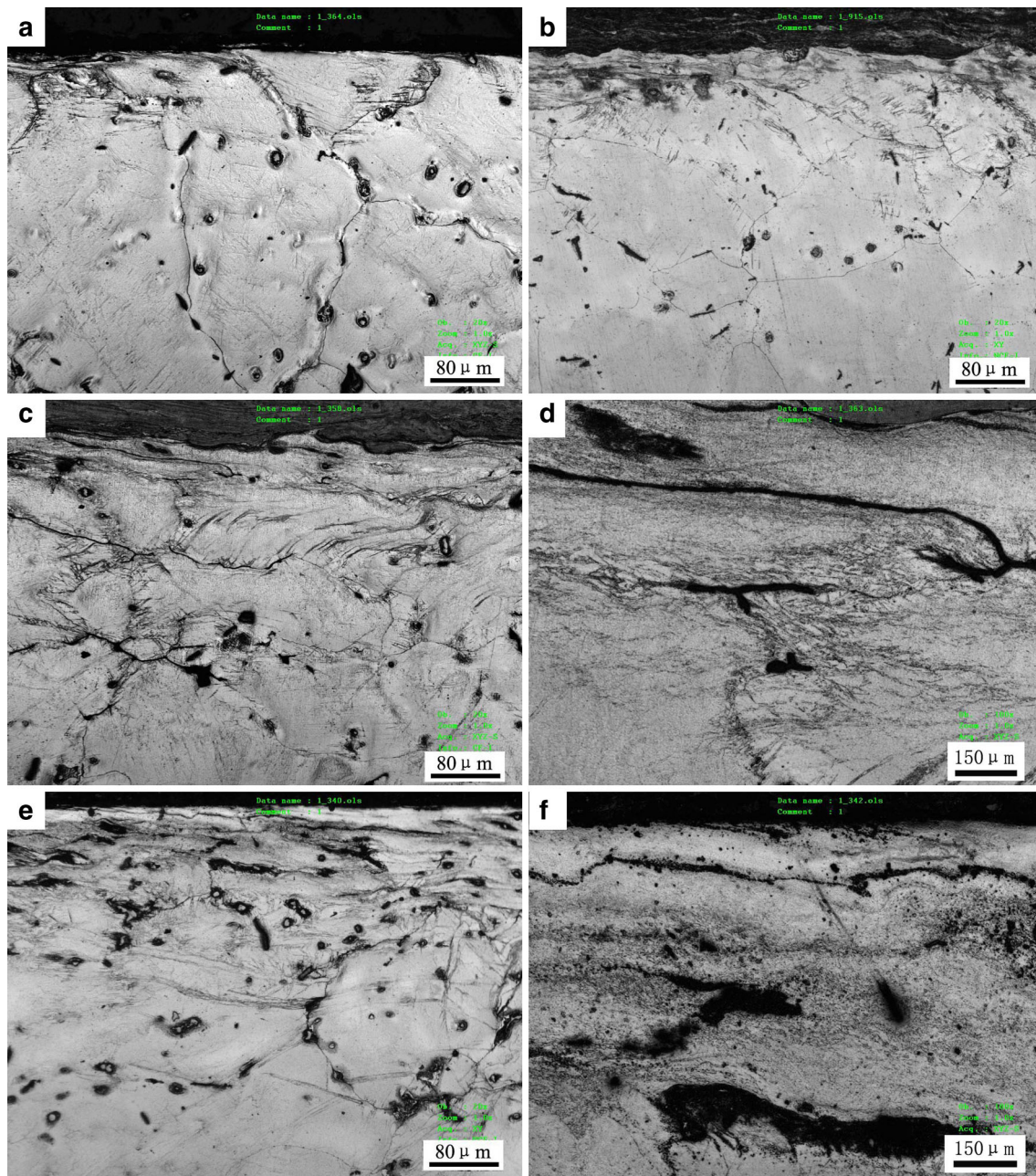


**Fig. 9** Cross-sectional microstructures of AZ31 alloy at different loads under 0.785 m/s: **a** 15 N, showing deformed top surface grains, **b** 70 N, showing increased twins, **c** 190 N, showing DRX zone, **d** 190 N, showing details of DRX zone, **e** 300 N, showing solidified zone, **f** 300 N, showing details of solidified zone

where  $T_0$  is the temperature of the heat sink where the heat flows,  $\mu$  is the coefficient of friction,  $F$  is the normal force on the pin,  $v$  is the sliding speed,  $A_n$  is the nominal contact area,  $\alpha$  is the fraction of the heat conducted into the pin,  $l_b$  is the mean diffusion distance,  $K_{mp}$  and  $K_{md}$  are the thermal conductivities of the pin and disc,  $a$  is the thermal diffusivity of steel and  $r_0$  is the radius of the pin.

The surface temperature as a function of applied load is plotted in Fig. 8. The thermal conductivity is taken as

87.4 J/ms at 25–300 °C, 75.5 J/ms at 300–500 °C, 68.9 J/ms at 500–630 °C for AZ31 alloy, and 41 J/ms for steel [23]. Surface temperature rise during dry sliding wear test can be divided into three regions i.e. from room temperature to DRX temperature, from DRX temperature to melting temperature, and above melting temperature. It can be seen that the surface temperature was lower than 100 °C within the load range of 5–360 N under 0.1 m/s, therefore, surface hardening could operate throughout the



whole applied load range. In contrast, surface temperatures were higher than 300 °C, i.e., the DRX temperature of AZ31 alloy within 120–240 N at 0.785 m/s and 70–120 N at 1.5 m/s. It suggests that DRX can fully develop in subsurfaces during dry sliding wear tests. Therefore, thermal softening suppressed the surface strain hardening effect and became the dominant factor affecting wear rate until occurrence of surface melting. In addition, the load ranges relating with regions of surface hardening, softening and melting in Fig. 6 agree well with their counterparts in calculated surface temperature versus applied curves.

### 3.4 Subsurface Microstructures

Figure 9 shows the subsurface microstructural evolution with applied load under 0.785 m/s sliding condition. Even at low load of 15 N, a deformation zone with depth of 85–120 µm was formed beneath worn surface, where a series of parallel fine twins lines originated from grain boundaries and extended into interior of the surface grains, as shown in Fig. 9a. Since magnesium and its alloy is a lack of slip systems, i.e., basal slip system, twinning is known to form easily to supplement for the slip systems during plastic deformation at room temperature [24, 25]. At 70 N, the deformation zone extended to 250 µm depth, and long lenticular twins widened in the grains and density of twins apparently increased (Fig. 9b). With increasing load to 190 N, a DRX zone with depth of about 30 µm occurred immediately beneath worn surface, no twins were observed apparently, followed by a 160 µm thick deformation zone in which the twins near the DRX zone were bent towards sliding direction (Fig. 9c). The details of DRX zone are clearly presented in Fig. 9d. The DRX grains mainly formed at boundaries with high density of twins. At high load of 320 N, a solidified zone with depth 20 µm thickness was formed, followed by the DRX zone with depth of 35 µm and the deformation zone with depth of 35 µm with less twins (Fig. 9e). High magnitude photograph of solidified zone exhibits formation of fine-grain microstructure (Fig. 9f). That is why re-solidified surface demonstrates a low level of hardness in Fig. 7, but still higher than hardness of as-received material. The subsurface microstructural evolution further supports the subsurface strain hardening arising from accumulation of plastic strain, thermal softening originating from DRX and surface melting. Therefore, a conclusion can be drawn that friction-induced strain hardening plays a dominant role in mild wear regime, while surface thermal softening originating from DRX and surface melting prevail in severe wear regime.

## 4 Conclusions

- Under the sliding speeds of 0.1, 0.785 and 1.5 m/s, the coefficient of friction of AZ31 alloy decreased with increasing applied load, and the wear rate increased in different manners with increasing applied load. At low sliding speed of 0.1 m/s, the mild wear regime prevailed throughout whole applied load range. At high sliding speeds of 0.785 and 1.5 m/s, mild wear regimes were restricted within certain limited load ranges of 5–120 N and 5–70 N, respectively.
- Even at a low load or after a short sliding distance, large plastic shear strain was found to accumulate in the near-surface region during dry sliding wear test. The large plastic strain region widened with increasing load and sliding distance.
- Friction-induced strain hardening accounted for the low slope of wear rate in mild wear regime, while surface softening originating from DRX and surface melting were dominant factors for the rapid wear in severe wear regime.
- In mild wear regime, with increasing applied load, deformation zone extended from top parts of surface grains to deep grains. In severe wear regime, when the wear behaviour transformed from severe plastic deformation into surface melting, the subsurface microstructure also transformed from DRX zone + deformation zone into the solidified fine grain zone + DRX zone + deformation zone.

**Acknowledgments** The authors thank the Project 985-automotive engineering of Jilin University and National Foundation of Doctoral Station (Grant No.20110061110031).

## References

1. Mordike B L, and Ebert T, *Mater Sci Eng A* **302** (2001) 37.
2. Avedesian M M, and Baker H, *Magnesium and Magnesium Alloys-ASM Specialty Handbook*, ASM International Materials Park (1999), p13.
3. Barnett M R, Keshavarz Z, and Beer A G, *Acta Materialia* **52** (2004) 5093.
4. Janik V, Yin D D, Wang Q D, He S M, Chen C J, Chen Z, and Boehlert C J, *Mater Sci Eng A* **528** (2011) 3105.
5. Kawamura Y, Hayashi K, Inoue A, and Masumoto T, *Mater Trans JIM* **42** (2001) 1172.
6. Inoue A, Matsusita M, Kawamura Y, Amiya K, Hayashi K, and Koike J, *Mater Trans JIM* **43** (2002) 580.
7. Habibnejad-Korayem M, Mahmudi R, Ghasemi H M, and Poole W J, *Wear* **268** (2010) 405.
8. Chen H and Alpas A T, *Wear* **246** (2000) 106.
9. El-Morsy A-W, *Mater Sci Eng A* **473** (2008) 330.
10. Taltavull C, Torres B, Lopez A J, and Rams J, *Wear* **301** (2013) 615.
11. Paddar P, Das A, and Sahoo K L, *Mater Des* **54** (2014) 820.

12. Anbu selvan S, and Ramanthan S, *Mater Des* **31** (2010) 1930.
13. Jungk J M, Michael J R, and Pasad S V, *Acta Materialia* **56** (2008) 1956.
14. Das S, Morale A T, and Alpas A T, *Wear* **268** (2010) 94.
15. Somekawa H, Meada S, Hirayama T, Mitsuoaka T, Inoue T, and Mukai T, *Mater Sci Eng A* **561** (2013) 371.
16. Yao B, Han Z, and Lu K, *Wear* **294–295** (2012) 438.
17. Nguyen Q B, Sim Y H M, Gupta M, and Lim C Y H, *Tribol Int* (2014), doi:[10.1016/triboint2014.02.024](https://doi.org/10.1016/triboint2014.02.024).
18. An J, Li R G, Lu Y, Chen C M, Xu Y, Chen X, and Wang L M, *Wear* **265** (2008) 97.
19. Wang S Q, Yang Z R, Zhao Y T, and Wei M X, *Tribol Lett* **38** (2010) 39.
20. Moore M A, and Douthwaite R M, *Metall Trans A* **7** (1976) 1833.
21. Tan J C, and Tan M J, *Mater Sci Eng A* **339** (2003) 124.
22. Mwembela A, Konopleva E B, and McQueen H J, *Scripta Materialia* **37** (1997) 1789.
23. Lim S C, and Ashby M F, *Acta Metallurgica* **35** (1987) 1.
24. Wonsiewicz B C, and Backofen W A, *Trans Metall Soc AIME* **239** (1967) 1422.
25. Yoshinaga H, and Horiuh R, *Mater Trans JIM* **4** (1963) 134.